NEUROPHYSIOLOGY

Mfsd2a and Spns2 are essential for sphingosine-1-phosphate transport in the formation and maintenance of the blood-brain barrier

Zhifu Wang[1,2]*, Yongtao Zheng[1]*, Fan Wang[1,3]*, Junjie Zhong[1], Tong Zhao[1], Qiang Xie[1], Tongming Zhu[1], Fukai Ma[1], Qisheng Tang[1], Bin Zhou[2†], Jianhong Zhu[1†]

To maintain brain homeostasis, a unique interface known as the blood-brain barrier (BBB) is formed between the blood circulation and the central nervous system (CNS). Major facilitator superfamily domain-containing 2a (Mfsd2a) is a specific marker of the BBB. However, the mechanism by which Mfsd2a influences the BBB is poorly understood. In this study, we demonstrated that Mfsd2a is essential for sphingosine-1-phosphate (S1P) export from endothelial cells in the brain. We found that Mfsd2a and Spinster homolog 2 (Spns2) form a protein complex to ensure the efficient transport of S1P. Furthermore, the S1P-rich microenvironment in the extracellular matrix (ECM) in the vascular endothelium dominates the formation and maintenance of the BBB. We demonstrated that different concentrations of S1P have different effects on BBB integrity. These findings help to unravel the mechanism by which S1P regulates BBB and also provide previously unidentified insights into the delivery of neurological drugs in the CNS.

INTRODUCTION

A specialized cerebrovascular structure isolates the brain parenchyma from the blood circulation; this structure is termed the "neurovascular unit" (NVU) and includes endothelial cells (ECs), pericytes, and astrocytes (*1*–*3*). Although the NVU is a complex unit, current research suggests that ECs are the core element of the blood-brain barrier (BBB) (*1*, *4*). ECs in brain capillaries are arranged in a single-cell layer between the blood and brain tissue to form tight junctions (TJs) and tightly control substance transportation. The permeability of the cerebral vascular endothelium is much lower than that of the peripheral tissues. Low permeability allows the endothelium to filter pathogens, neural toxins, blood cells, and most macromolecular compounds (such as albumin). Substance transport from the blood to the brain parenchyma mainly depends on transcellular transport because of the sophisticated structure of NVU and TJs in the endothelium, and caveolin-1 (Cav-1) is critical for transcytosis in ECs (*5*, *6*). Growing evidence suggests that multifactorial disorders of the central nervous system (CNS) are associated with BBB breakdown (*7*–*10*). Therefore, the mechanisms by which multiple factors influence the maintenance of the BBB also potentially contribute to neurological disorders.

Recent studies have demonstrated that major facilitator superfamily (MFS) domain-containing 2a (Mfsd2a) is a critical transmembrane liquid transporter for the maintenance of the BBB (*11*). Both Mfsd2a and Mfsd2b are orphan transporters and are classified as subtypes of the MFS according to sequence similarity and phylogenetic closeness. Another study of Mfsd2a as a docosahexaenoic acid (DHA) transporter was also conducted recently (*12*, *13*). Subsequently, two investigations reported that both lethal and nonlethal hereditary microcephaly are associated with the mutation of the Mfsd2a gene (*14*, *15*). These spurred studies that aimed to obtain novel insights into the relationship between BBB breakdown and hereditary diseases in the CNS. However, the mechanism by which Mfsd2a manipulates the BBB remains to be further resolved (*16*), and it is unknown whether this process is only determined by DHA. Sphingosine-1-phosphate (S1P) is a biologically active lipid mediator that plays a key role in regulating cell migration, adhesion, survival, and proliferation (*17*). S1P is produced intracellularly from sphingosine by the phosphorylation of sphingosine kinases Sphk1 and Sphk2 (*18*). S1P signaling is achieved by its interaction with intracellular targets or autocrine/paracrine transporters, which activates its cell surface receptors [S1P receptors (S1PRs) and S1P1 to S1P5] (*19*). As an intracellular second messenger (*20*), S1P must transmit its signals through specific receptors during development. A lack of S1P1 causes impaired vascular maturation and severe bleeding, leading to embryonic death (*21*). Although S1P is essential for peripheral vascularization and organ development, it is also indispensable in brain development (*22*). There was a study that reported that conditionally knocking out S1P1, which is an important receptor for S1P, can induce high permeability in ECs (*23*).

In this study, we found that Mfsd2a, which is a subtype of an MFS protein, is an essential element for S1P export from cerebral ECs and substantially increases the transport of S1P by binding to S1P. We also found that a high concentration of S1P in the microenvironment helps the vascular endothelium maintain low permeability, which is essential for the formation and maintenance of the BBB.

RESULTS

Interference with S1P in vivo leads to the gradual breakdown of the BBB

S1P modulates multiple functions in vivo through its binding to five different S1PRs known as S1P1 to S1P5. A recent study demonstrated

[1]Department of Neurosurgery, Huashan Hospital, Institute of Brain Science, State Key laboratory of Medical Neurobiology, Shanghai Key Laboratory of Brain Function and Regeneration, Shanghai Medical College, Fudan University, No.12 Urumqi Mid Road, Shanghai 200040, China. [2]State Key Laboratory of Cell Biology, CAS Center for Excellence in Molecular Cell Science, Shanghai Institute of Biochemistry and Cell Biology, Chinese Academy of Sciences (CAS), University of CAS, Shanghai, China. [3]Department of Neurology, Peking University Third Hospital, Beijing, China.
*These authors contributed equally to this work.
†Corresponding author. Email: zhoubin@sibcb.ac.cn (B.Z.); jzhu@fudan.edu.cn (J.Z.)

that the interspacing of ECs became larger in the brain after S1P1 was conditionally knocked out (*23*). Fingolimod (FTY720) is an antagonist of S1PR subtypes that blocks the binding of S1P to S1P1 (*24*, *25*). Wild-type mice were continuously treated with FTY720 by intraperitoneal injection to investigate whether S1P influences the BBB (fig. S1A). We found that the BBB was disrupted during FTY720 administration, which peaked on the sixth day of dosing (D6) (fig. S1C). The brains of D1 to D8 mice were harvested to measure BBB leakage. Our data show that different concentrations of FTY720 result in different degrees of impairment in the BBB (fig. S1, B and C) and that BBB breakdown is a gradual process. These results are in line with the features of the BBB described previously (*2*), indicating that S1P is a potential factor involved in the maintenance of the BBB.

Mfsd2a deficiency causes the insufficient transport of S1P in the brain parenchyma, resulting in BBB breakdown

To investigate S1P transport and BBB leakage in Mfsd2a-deficient mice and to show the expression of Mfsd2a in the brain, the cycling recombination enzyme-estrogen receptor ($CreER^{T2}$) gene was knocked in to replace exon 1 of the Mfsd2a gene (fig. S2A), which has been previously reported (*6*). We tested the mRNA and protein levels of Mfsd2a in the cerebral cortex to verify the absence of Mfsd2a in $Mfsd2a^{CreERT2/CreERT2}$ mice (fig. S2, B and C). We also found that the brains of homozygous mice were substantially smaller than those of heterozygotes (fig. S2D). Then, a 10-kDa dextran tracer was injected through the left ventricle to test the permeability of the cerebral vessels, and the dextran tracer permeated the brain parenchyma in homozygous mice, which indicated the leakage of the BBB. The phenotypes of the $Mfsd2a^{CreERT2/CreERT2}$ mice are consistent with those found in previous studies (fig. S2, E to G) (*11*). In addition, the results of behavioral tests for homozygous mice were similar to those of $Mfsd2a^{-/-}$ mice (fig. S3) (*12*). Lineage tracing in Mfsd2a-$CreER^{T2}$ mice shows that the Mfsd2a gene is highly expressed in ECs in the brain (fig. S3A). In addition, behavioral tests were also performed to compare the homozygous mice and the heterozygous mice. The $Mfsd2a^{CreERT2/CreERT2}$ mice exhibited dyskinesia and anxiety (fig. S3), which was similar to what was observed in Mfsd2a-deficient mice (*12*). Consequently, the homozygous mice were identified as Mfsd2a-deficient mice ($Mfsd2a^{-/-}$ mice).

There is no doubt that Mfsd2a is a critical switch in the BBB, but studies on the role of DHA deficiency in BBB breakdown are contradictory. A recent study proposed that the absence of DHA promotes Cav-1–mediated vesicular transport (*6*). However, there is sufficient evidence to support that an extremely low DHA diet in postnatal mice did not lead to the increased permeability of a 30-kDa dextran tracer and other proteins, including albumin (*26*). Therefore, we tested the permeability for albumin in cerebral ECs by Evans blue staining staining staining. Cav-1 mediates the transcytosis of albumin in cerebral ECs (*27*), which, at least, indicates that DHA is not the only factor that regulates the BBB.

In addition, we found that the permeability of cerebral vessels in $Mfsd2a^{-/-}$ mice to Evans blue staining staining staining was much lower than that in D6 mice (Fig. 1, A and B), which suggests that the BBB in Mfsd2a-deficient mice is disrupted incompletely. The pattern of BBB leakage in D4 mice is quite similar to the phenotype observed in $Mfsd2a^{-/-}$ mice (Fig. 1D), including permeability to Evans blue staining and a 10-kDa dextran tracer (Fig. 1, E and F). To determine whether Mfsd2a influences the export of S1P in the brain, we subsequently measured the concentration of S1P in the cytoplasm and extracellular matrix (ECM). The mass spectrometry (MS) and enzyme-linked immunosorbent assay (ELISA) data showed a notable reduction in the S1P concentration in the ECM in Mfsd2a-deficient brains, while there was no substantial difference in the S1P concentration in the cytoplasm (Fig. 1, G and H). We demonstrated that a low concentration of S1P in the ECM causes the incomplete breakdown of BBB, indicating that transcytosis in the brain is not only predominantly mediated by Mfsd2a but also that more evidence is required to determine whether S1P directly affects the maintenance of the BBB.

S1P is exported by Spns2 in brain ECs, and Mfsd2a supports improved efficiency in S1P transport

Although the transport of S1P in the Mfsd2a-deficient brain is reduced, the S1P concentration in the ECM in the brain is still at a high level, indicating that Mfsd2a is involved in the transport of S1P but does not serve as a major transporter for S1P. A recent investigation reported that S1P is not a competitor for Mfsd2a, which supports this conclusion. Spinster homolog 2 (Spns2) has been identified as the major transporter for S1P in ECs (*28*, *29*). We subsequently tested the expression of Spns2 in the brain to determine whether Spns2 is specifically expressed in ECs. To show that the insufficient export of S1P can lead to BBB breakdown, we generated Spns2–short hairpin RNA (shRNA) (Table 1) to inhibit the expression of Spns2. An adeno-associated virus (AAV) containing Spns2-shRNA was injected into the corpus callosum to transfect the cerebral cortex (Fig. 2, A to C). To determine that Mfsd2a can improve S1P transport, we transfected the human embryonic kidney (HEK) 293 cell line with plasmids that expressed human Spns2 or/and Mfsd2a (fig. S4, A and B). Double-positive cells ($Spns2^+$ $Mfsd2a^+$) have more efficient S1P uptake than $Spns2^+$ cells, showing that Mfsd2a can lead to a remarkable improvement in S1P transport (fig. S4C). Consistent with previous studies (*12*), there is no significant difference in the uptake efficiency in $Mfsd2a^+$ cells (fig. S4C), indicating that Mfsd2a has no capability to transport S1P directly.

The results obtained by MS showed that the S1P concentration in the ECM was markedly decreased and was lower than that in Mfsd2a-deficient mice after Spns2 was knocked down (Fig. 2E), indicating that Spns2 is the major transporter of S1P in brain ECs. Furthermore, the decreased concentration of S1P in the ECM leads to the loss of TJs in brain ECs (Fig. 2C) (*30*), and a similar phenotype was also found in brain ECs in D6 mice, whereas TJs are normally present in $Mfsd2a^{-/-}$ mice and D4 mice (fig. S5, A to D). Moreover, compared with ECs in $Mfsd2a^{-/-}$ mice, the ECs in the Spns2-deficient cortex had a higher permeability to Evans blue staining (Fig. 2F), which is similar to that observed in the brains of D6 mice. These data further suggest that adequate S1P concentrations are essential for the maintenance of the BBB. Last, whether gene-deficient mice or D4/D6 mice have typical pericytes around the brain ECs was determined (fig. S5, E and F).

Unexpectedly, injecting S1P directly to the brain can reverse the BBB breakdown caused by Spns2 deficiency (Fig. 2G). We next tested the permeability of brain ECs to a 10-kDa dextran tracer. The 10-kDa dextran tracer could not penetrate into the brain parenchyma, indicating the recovery of the BBB (Fig. 2, H and I). This finding provides new evidence to support the conclusion that a high S1P concentration in the ECM is critical for maintaining the BBB.

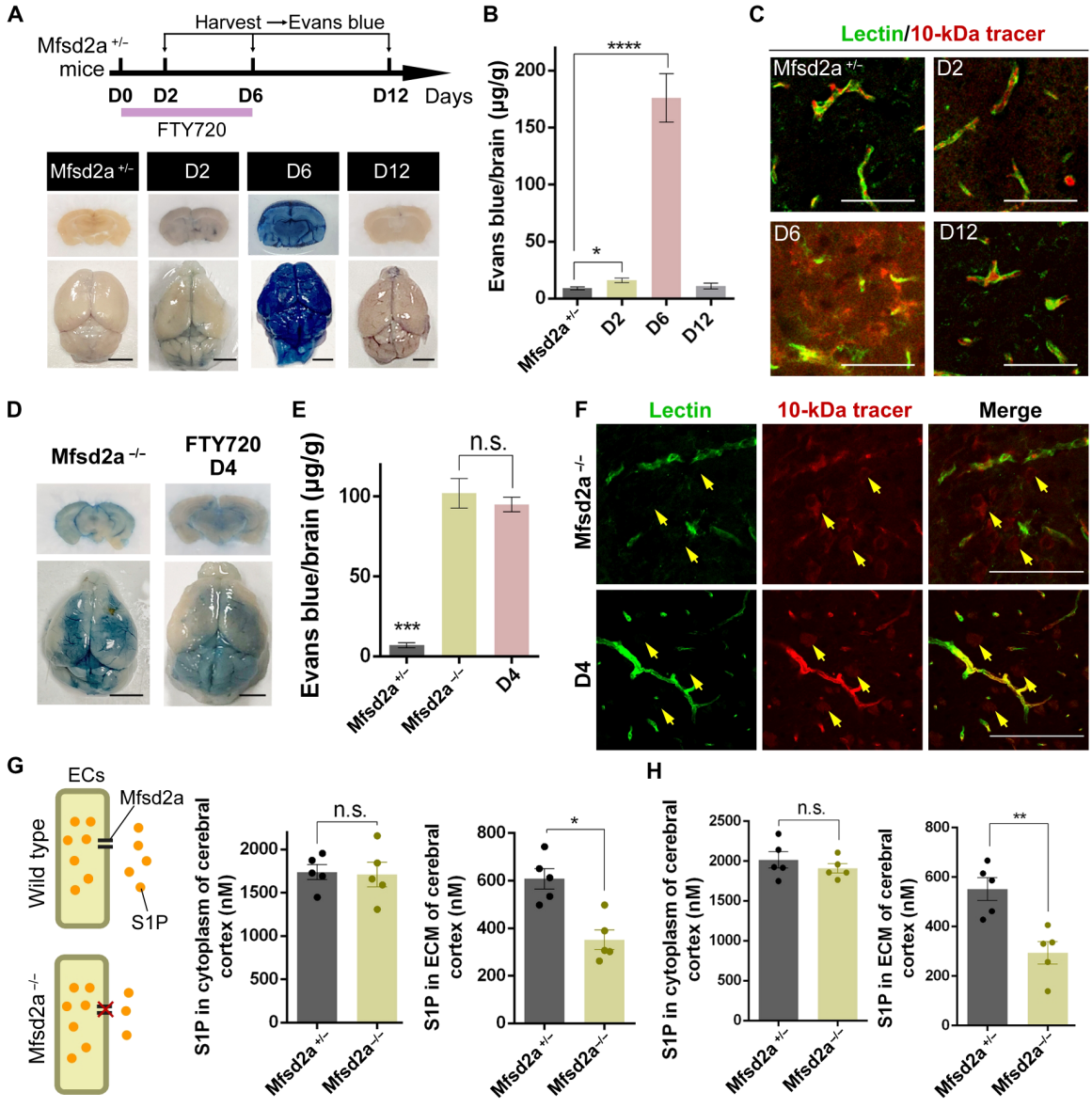

Fig. 1. Mfsd2a deficiency causes insufficient transport of S1P in the brain parenchyma, resulting in BBB breakdown. The S1P concentration in the ECM in the brain is reduced in Mfsd2a$^{-/-}$ mice. (**A**) Strategy used for FTY720 injection and Evans blue examination of the BBB ($n = 5$ male mice per group). (**B**) Evans blue examination showed that the BBB was disrupted gradually by FTY720, and the BBB recovered after discontinuing FTY720. (**C**) The tracer (red) was confined to the capillaries (green) in Mfsd2a$^{+/-}$ mice and D12 mice, and D6 mice showed higher permeability than D2 mice ($n = 3$ male mice per group). (**D**) Whole-mount images showed that Mfsd2a$^{-/-}$ mice had a pattern of permeability similar to that in D4 mice ($n = 6$ male mice per group). (**E**) Quantification of Evans blue staining showed similar Evans blue leakage in the brain parenchyma in Mfsd2a$^{-/-}$ mice and D4 mice. (**F**) Both Mfsd2a$^{-/-}$ and D4 mice showed tracer leakage (yellow arrows, $n = 3$ male mice per group). (**G** and **H**) Concentrations of total S1P in the cytoplasm and the ECM; the S1P concentration in the ECM was reduced in the Mfsd2a$^{-/-}$ mice compared with Mfsd2a$^{+/-}$ mice, but there was no significant difference in the S1P concentration in the cytoplasm (G, MS tests; H, ELISA tests). Scale bars: 4 mm in A and D; 100 μm in C and F. Error bars: SEM. Significance determined by Students *t*-test: ****$P < 0.0001$, ***$P < 0.001$, **$P < 0.01$, *$P < 0.05$, n.s. $P > 0.05$. Photo credit: Zhifu Wang, State Key Laboratory of Medical Neurobiology, the Institutes of Brain Science and the Collaborative Innovation Center for Brain Science, Shanghai Medical College, Fudan University.

Table 1. AAV: AAV9-Spns2-RNAi; AAV9-S1P1-RNAi (Shanghai GeneChem).

	5′	STEM	Loop	STEM	3′
Spns2-RNAi	ACCGG	TACCAAGAACACACGCACATT	CTCGAG	AATGTGCGTGTGTTCTTGGTA	TTTTT
S1P1-RNAi	TCTAAAAAA	CTGACTTCAGTGGTGTTCA	CTCGAG	TGAACACCACTGAAGTCAG	C
Control	CGCTGAGTACTTCGAAATGTC				

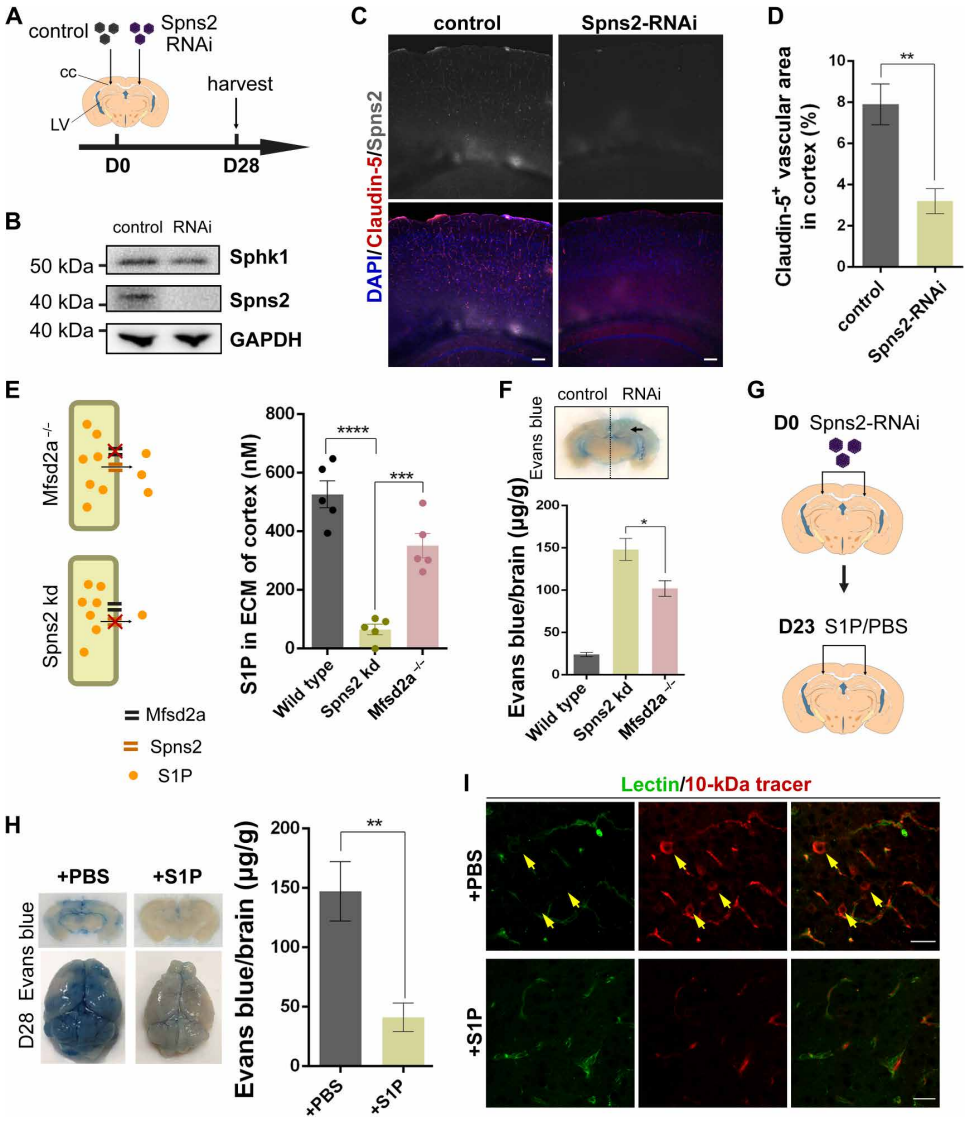

Fig. 2. Spns2 is the major transporter of S1P. Compared to Mfsd2a deficiency, Spns2 deficiency results in a decreased S1P concentration and the increased permeability of the BBB. (**A**) Strategy used for Spns2-RNAi transfection. (**B**) Western blot analysis showed that Spns2 was knocked down at D28 in the cortex when compared to that in the contralateral cortex ($n = 3$ male mice per group). (**C**) Immunostaining for Spns2 and claudin-5 showed that the expression of claudin 5 was downregulated after Spns2 inhibition ($n = 3$ male mice per group). (**D**) Quantification of the area of claudin 5-positive ECs in cortex ($n = 5$ male mice per group). (**E**) Quantitative analysis indicated that the S1P concentration in the ECM in the cortex of Spns2- deficient mice was lower than that in Mfsd2a-deficient mice. (**F**) The cerebral cortex was permeable to Evans blue (black arrowhead) when Spns2 was knocked down ($n = 3$ male mice per group). (**G** and **H**) S1P or PBS was added in situ at 23 days post AAV injection; whole-mount images showed that additional S1P decreased Evans blue leakage, whereas PBS had no effect; quantification of Evans blue showed that compared with PBS, additional S1P had a significant effect on BBB breakdown ($n = 4$ male mice per group). (**I**) Immunostaining showed that the tracer (red) was confined to the vessels (green) after adding S1P, but tracer leaked (yellow arrows) from the vessels after adding PBS. ($n = 3$ male mice per group). cc, corpus callosum; LV, lateral ventricle. Scale bars: 100 μm in C; 50 μm in I. Error bars: SEM. Significance determined by Students *t*-test: $^{***}P < 0.001$, n.s. $P > 0.05$. Photo credit: Fan Wang, State Key Laboratory of Medical Neurobiology, the Institutes of Brain Science and the Collaborative Innovation Center for Brain Science, Shanghai Medical College, Fudan University.

The S1P signaling pathway is crucial for the maintenance of the BBB

As an antagonist of S1P, FTY720 also affected the immune system in our experiments (*31*). To rule out interference from immune cells in peripheral blood, we intended to test the integrity of the BBB after local inhibition of the S1P/S1P1 pathway by stereotactic injection (Fig. 3A). Previous studies have convincingly demonstrated that S1P1 is an important receptor in ECs for S1P (*32*, *33*). The S1P1 protein is extensively expressed in multiple cells in the brain, including ECs (fig. S7B). Unexpectedly, the BBB can be disrupted by blocking S1P receptors. An AAV containing S1P1–RNA interference (RNAi) (Table 1) was designed to knock down S1P1 expression. The hippocampus, which is large enough and does not affect the peripheral nuclei, was selected as the target because of its high contrast with the peripheral brain parenchyma (Fig. 3A). Compared with its expression in the vehicle, there was a substantial down-regulation of S1P1 in the contralateral hippocampus (Fig. 3, B and C).

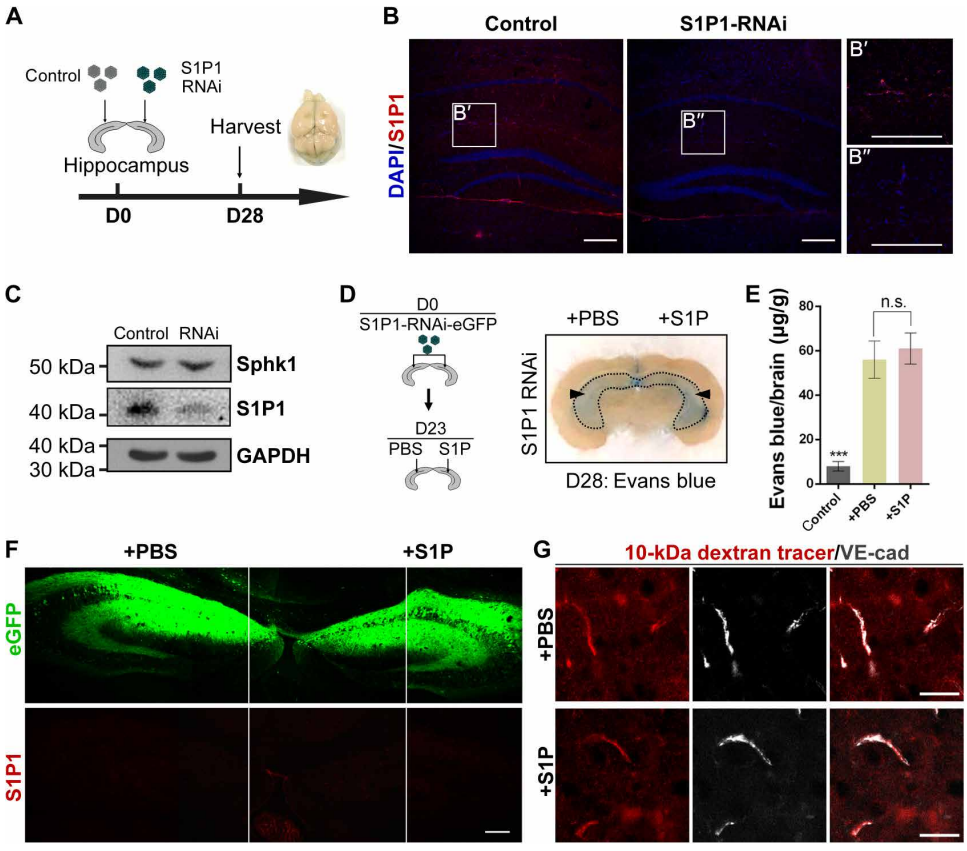

Fig. 3. The S1P signaling pathway is crucial for the maintenance of the BBB. Knock down of S1P1 in the hippocampus led to BBB breakdown. (**A**) Strategy used for S1P1-RNAi transfection. (**B**) Immunostaining for S1P1 showed that the expression of S1P1 was inhibited after RNAi transfection. (**C**) Western blot showing that S1P1 knockdown had no substantial effect on the expression of Sphk1 at D28. (**D**) S1P or PBS was added in situ at 23 days post AAV injection; Evans blue leakage was confined to the hippocampus (black arrowheads). (**E**) Quantification of Evans blue staining showed that additional S1P had no effect on BBB breakdown. (**F**) The inhibition of S1P1 was not affected by additional PBS or S1P. (**G**) The tracer penetrated into the brain parenchyma, indicating that the BBB did not recover after adding S1P. Scale bars: 200 μm in B and F; 100 μm in G. Error bars: SEM. Significance determined by Students *t*-test: ***$P < 0.001$, n.s. $P > 0.05$. Each image is representative of three individual male mice. Photo credit: Fan Wang, State Key Laboratory of Medical Neurobiology, the Institutes of Brain Science and the Collaborative Innovation Center for Brain Science, Shanghai Medical College, Fudan University.

Although we cannot perform a conditional knockout in the endothelium, the experimental results are consistent with the results of a previously reported conditional knockout experiment (*23*); therefore, we suggest that the inactivation of S1P1 in ECs causes BBB breakdown. Then, we knocked down the S1P1 gene in the bilateral hippocampus, and 200 nl of S1P (1 mM) was injected in situ into the right hippocampus at 23 days after AAV injection (D23), while 200 nl of phosphate-buffered saline (PBS) was injected into the contralateral hippocampus (Fig. 3D). We found that the ECs in the brain were permeable to Evans blue only in the hippocampus after inhibiting S1P1, indicating that the BBB was locally disrupted (Fig. 3, D and E). The expression of S1P1 was not affected by S1P or PBS (Fig. 3F). There was no significant difference in the permeability of the brain endothelium exposed to S1P to Evans blue staining and a 10-kDa dextran tracer compared with endothelium exposed to PBS, and additional S1P did not contribute to the recovery of the BBB when S1P1 was blocked (Fig. 3, E and G). These results suggest that the interaction between S1P and S1P1 in brain ECs rather than that in peripheral immune cells supports the maintenance of the BBB.

An S1P-enriched microenvironment is required specifically to decrease the permeability and transcytosis in brain ECs

Our data show that different concentrations of S1P have different effects on the BBB, and we next investigated the mechanism by which S1P in the ECM induces ECs to maintain the BBB. Recent studies have shown that Mfsd2a deficiency stimulates transcellular vesicular transport in brain ECs and then disrupts the BBB (*6*, *34*), which is in line with the results that show that Evans blue staining penetrates into the brain parenchyma in Mfsd2a$^{-/-}$ mice. We then tested the expression of genes involved in transcytosis, but we found no significant differences in the expression of these genes in the Mfsd2a$^{-/+}$ and Mfsd2a$^{-/-}$ mice; however, the expression of tubulin was down-regulated in Mfsd2a$^{-/-}$ mice, indicating increased BBB permeability (Fig. 4A). We also found the increased expression of the S100 calcium-binding protein A8 (S100A8, Mrp8) in ECs in Mfsd2a$^{-/-}$ mouse brains. S100A8 can combine with another calcium-binding protein, S100A9 (also known as Mrp14), to form calprotectin, which is an S100A8-S100A9 complex (*35*, *36*). Both calprotectin and S100A8 are endogenous ligands of Toll-like receptor 4 (TLR4) (*35*, *37*). Growing evidence shows that additional

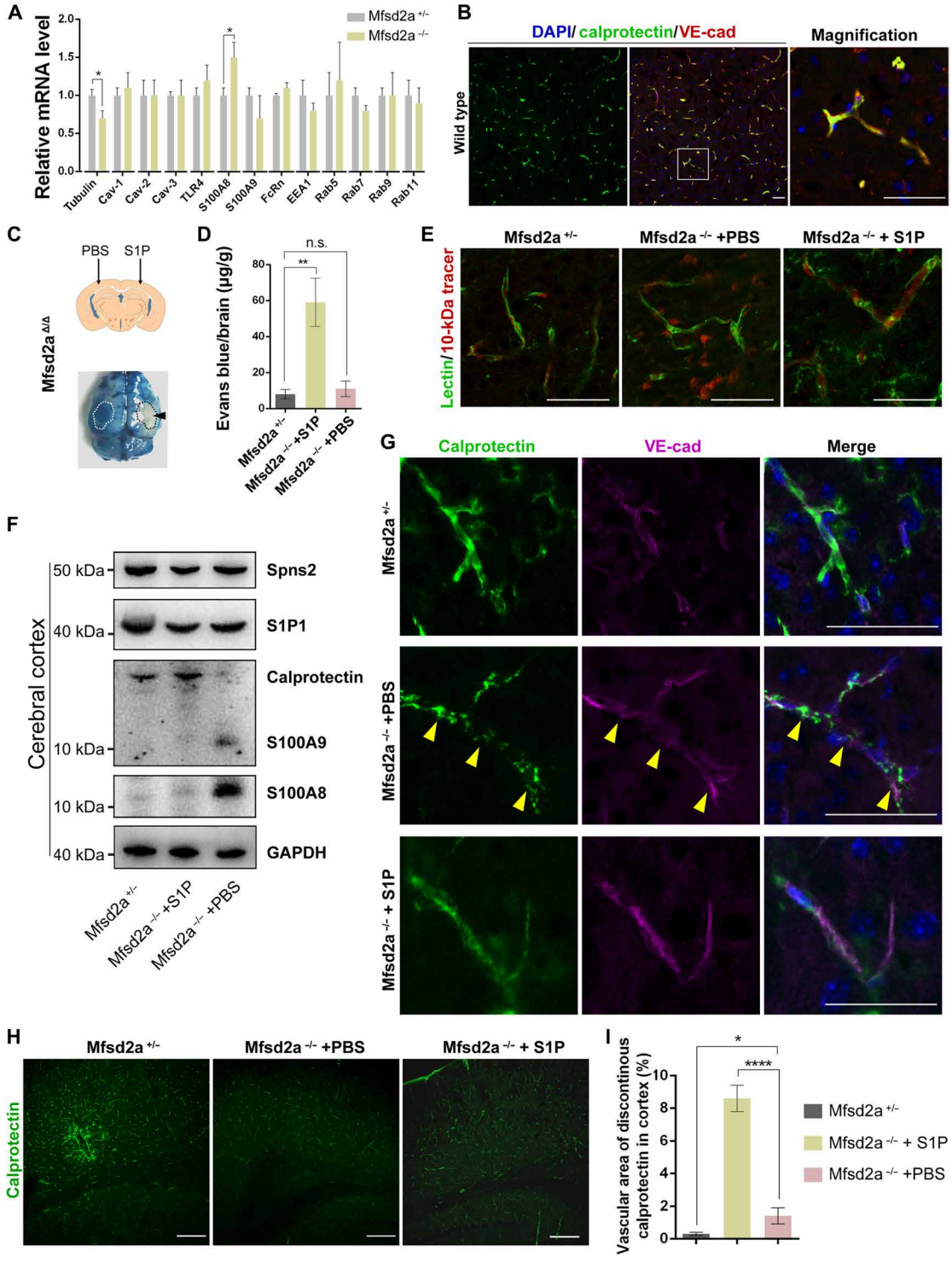

Fig. 4. A S1P-enriched microenvironment improves the stability of the S100A8/A9 complex in brain ECs. (**A**) Quantitative RT-PCR (qRT-PCR) analysis of transcytosis-related genes showed that brain ECs showed increases in S100A8 in Mfsd2a-deficient mice. (**B**) Immunostaining for calprotectin and VE-cad showing that brain ECs express calprotectin. (**C** and **D**) Whole-mount images and quantification showed that additional S1P decreased Evans blue leakage in Mfsd2a$^{-/-}$ mice. (**E**) The tracer was restricted to the capillaries after S1P injection. (**F**) Western blotting (Native-PAGE) showed that S100A8 was upregulated and calprotectin dissociated in ECs sorted from Mfsd2a-deficient mouse cortex; additional S1P reversed this phenotype. (**G**) Immunostaining for calprotectin and VE-cad showing the discontinuous distribution of calprotectin in ECs in Mfsd2a-deficient mouse cortex, and the distribution of calprotectin returned to normal after S1P injection. (**H**) Immunostaining for calprotectin in the cortex. (**I**) Quantitative analysis of the area of discontinuous calprotectin distribution. in cortical ECs. Scale bars: 100 μm in B; 50 μm in E and G; 200 μm in H. Error bars: SEM. Significance determined by Students *t*-test: ****$P < 0.0001$, ***$P < 0.001$, **$P < 0.01$, *$P < 0.05$, n.s. $P > 0.05$. Each result is representative of three individual mice. Photo credit: Fan Wang, State Key Laboratory of Medical Neurobiology, the Institutes of Brain Science and the Collaborative Innovation Center for Brain Science, Shanghai Medical College, Fudan University.

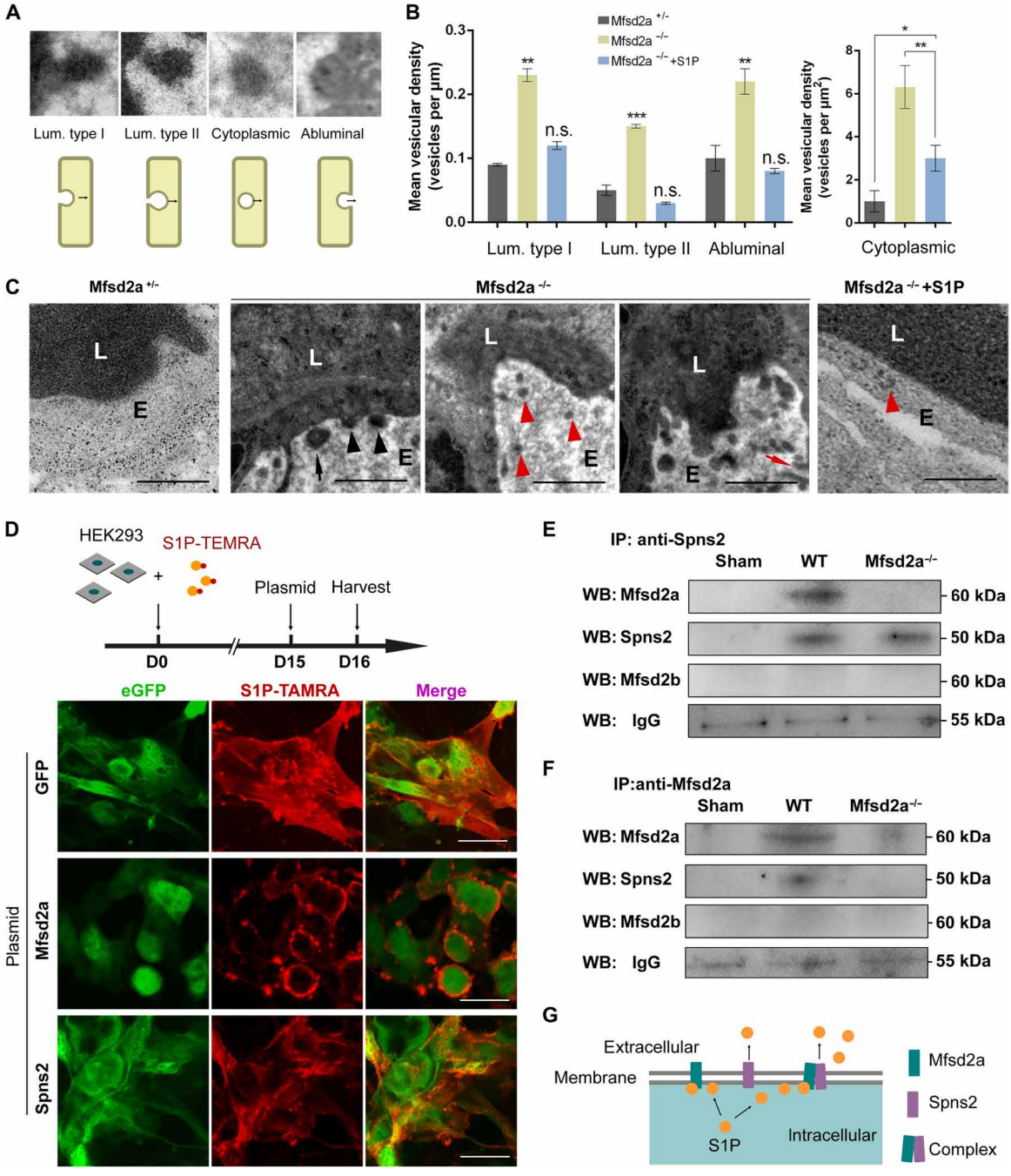

Fig. 5. A S1P-enriched microenvironment is required specifically to decrease the permeability and transcytosis in brain ECs. (**A**) Endothelium contained many vesicles of four types: Lum. type I [black arrowheads in (C)], Lum. type II [black arrows in (C)], Cytoplasmic [red arrowheads in (C)], and Abluminal [red arrows in (C)]. (**B**) Vesicular density quantification showed that additional S1P suppressed the transcytosis in Mfsd2a$^{-/-}$ mice [as shown in (C)]. (**C**) The transcytosis of adult Mfsd2a$^{-/-}$ mice injected with HRP was significantly increased. In wild-type littermates and Mfsd2a$^{-/-}$ mice with added S1P, HRP activity is confined to the lumen and there are no HRP-filled vesicles. (n = 3 mice per group) (**D**) HEK293 cells were incubated with S1P-TAMRA for fifteen days and then transfected with vehicle, Mfsd2a or Spns2 at D15. The fluorescence images showed that S1P (red) was enriched around the membrane after transfecting Mfsd2a. (**E** and **F**) Immunoprecipitation (IP) showed that Mfsd2a and Spns2 form protein complexes in brain ECs. (**G**) Schematic showing the mechanism of S1P transport by Mfsd2a and Spns2 in ECs of brain. L, lumen; E, endothelium. WT: wild-type. Scale bars: 500 nm in (C); 20 μm in (D). Error bars: SEM. Significance determined by Students t-test: ***P < 0.001, **P < 0.01, n.s. P > 0.05.Photo Credit: Zhifu Wang, State Key Laboratory of Medical Neurobiology, the Institutes of Brain Science and the Collaborative Innovation Center for Brain Science, Shanghai Medical College, Fudan University.

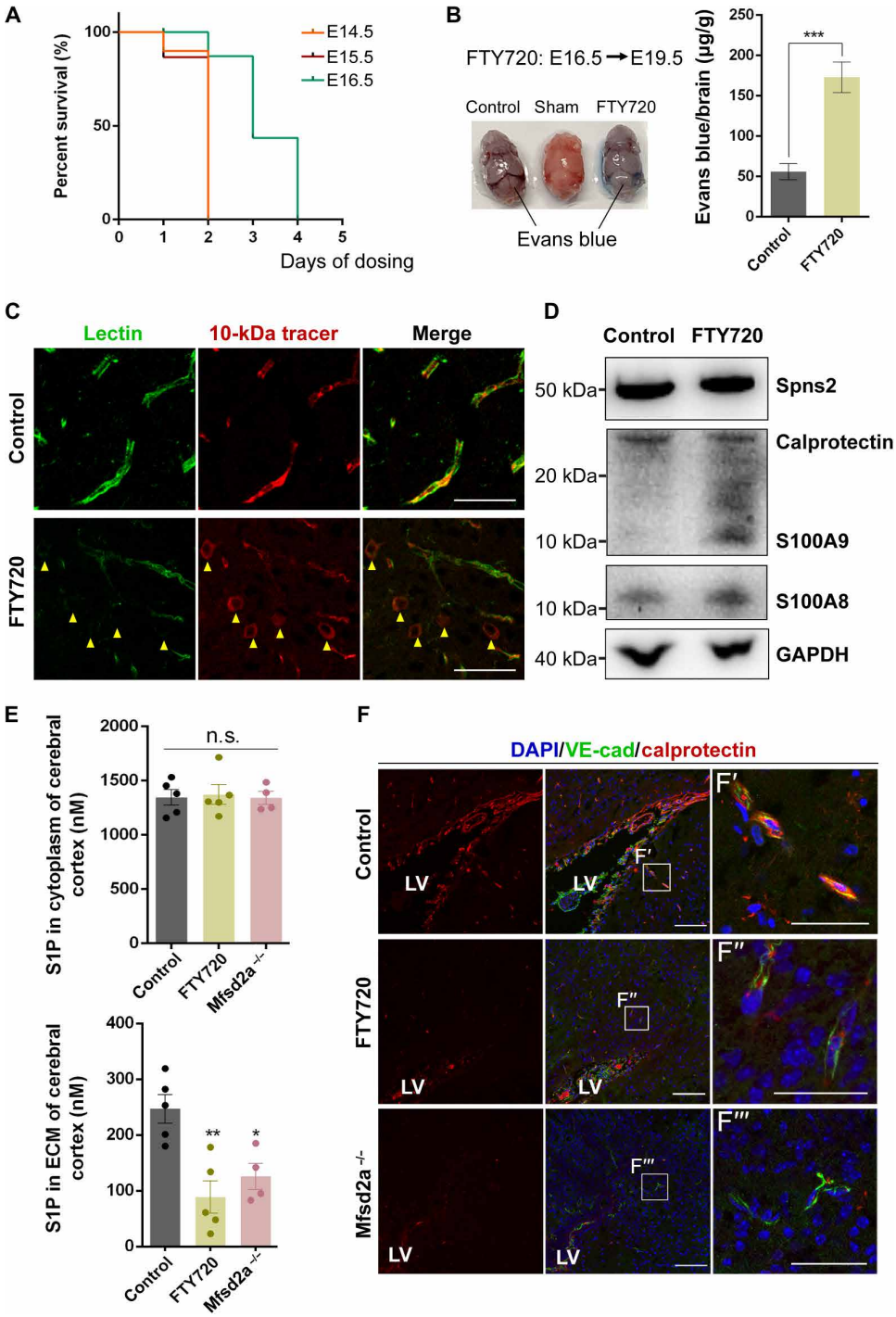

Fig. 6. S1P influences the formation of the BBB in embryos. Both FTY720 D3 and Mfsd2a$^{-/-}$ embryos showed BBB breakdown. (**A**) Survival analysis of wild-type embryos after FTY720 injection. ($n = 11$ embryos per group). (**B**) Quantification of Evans blue in embryonic brains showing that FTY720 interfered with BBB integration ($n = 5$ embryos per group). (**C**) Leakage of the tracer (yellow arrowheads) from the vessel lumen in an embryonic brain after dosing with FTY720 ($n = 3$ embryos per group). (**D**) Western blot showing that a proportion of calprotectin dissociated into S100A8 and S100A9 after FTY720 injection ($n = 3$ embryos per group). (**E**) Quantitative analysis showed that FTY720 had no effect on S1P concentration in embryonic brains, whereas Mfsd2a deficiency led to a reduction in S1P concentration in the ECM. (**F**) Immunostaining for calprotectin and VE-cad showing the discontinuous distribution of Calprotectin in both dosed embryos and Mfsd2a$^{-/-}$ embryos ($n = 3$ embryos per group). Scale bars: 80 μm in C; 200 μm in F; 100 μm in F′-F‴. Error bars: SEM. Significance determined by Students *t*-test: ***$P < 0.001$, *$P < 0.05$, n.s. $P > 0.05$. Photo credit: Fan Wang, State Key Laboratory of Medical Neurobiology, the Institutes of Brain Science and the Collaborative Innovation Center for Brain Science, Shanghai Medical College, Fudan University.

S100A8/A9 or TLR4 activation can stimulate transcytosis in ECs and disrupt the endothelial barrier (*38*–*40*). Our data show that calprotectin is specifically expressed in ECs in the brain (Fig. 4B and fig. S7). To determine the association between the abnormal expression of S100A8 and the lack of S1P, we injected S1P into the cerebral cortex by stereotactic injection. The addition of S1P decreases leakage in the BBB in Mfsd2a$^{-/-}$ mice (Fig. 4, C to E), further demonstrating that Mfsd2a deficiency leads to the insufficient export of S1P in the brain. Moreover, the expression of S100A8 was substantially down-regulated after adding S1P to the brain parenchyma (Fig. 4F). We found that the pattern of calprotectin/S100A9 distribution in brain ECs is completely different in Mfsd2a$^{-/+}$ and Mfsd2a$^{-/-}$ mice. Calprotectin/S100A9 is more discontinuously distributed in brain ECs in Mfsd2a$^{-/-}$ mice than in those in Mfsd2a$^{-/+}$ mice (Fig. 4G). This is likely because the abnormal S100A8/A9 complex interferes with the expression of S100A8 (*37*). The distribution of calprotectin was normalized after S1P treatment (Fig. 4, H and I). Similar results were also shown in Spns2 and S1P1 knockdown models (fig. S8). In summary, we cannot identify the cause of the stabilization of calprotectin but did reveal the close correlation between S1P and S100A8/A9 in brain ECs, which leads to the increased permeability of ECs.

Mfsd2a and Spns2 form a protein complex to promote S1P transport in brain ECs

To further demonstrate that the S1P-enriched microenvironment is required for BBB maintenance, we observed transcellular trafficking of ECs by electron microscopy. The cerebral cortex of horseradish peroxidase (HRP)–injected mice was collected for imaging; electron micrographs showed the electron-dense product that filled the lumen, by which we revealed the process of transcytosis (Fig. 5A). The HRP reaction product in Mfsd2a$^{-/-}$ mice was observed in vesicles invaginated from the luminal membrane and exocytosis in the extraluminal plasma membrane but was observed less in mice supplemented with S1P (Fig. 5, B and C).

Our findings support that a high concentration of S1P is critical for the maintenance of the BBB. However, the mechanism of S1P transport in brain ECs is unknown. Therefore, we sought to determine the mechanism by which Mfsd2a promotes S1P transport. Mfsd2a and Mfsd2b share ~60% similarity in sequence. Therefore, it is critical to identify the role Mfsd2b plays in S1P transport in ECs of the brain. But there is quite low expression of Mfsd2b in the brain (fig. S9, A and B), and Mfsd2b deficiency cannot lead to BBB breakdown (fig. S9C), indicating a minimal effect of Mfsd2b on S1P transport in the endothelium of the brain.

We found that the Mfsd2a can trap S1P in membrane (Fig. 5D and fig. S9, D and E). The negatively charged phosphate of S1P can bind to Mfsd2a, whereas S1P does not have the choline portion required for transport by Mfsd2a, indicating that the choline portion is important for the conformational change of Mfsd2a. Moreover, our results suggest that Mfsd2a and Spns2 can form a protein complex in brain ECs (Fig. 5, E and F). Together, we suppose that these two properties of Mfsd2a are critical for the improvement of S1P transport efficiency, S1P binds to Mfsd2a, and then is transported by Spns2 (Fig. 5G). Furthermore, we demonstrate that BBB breakdown caused by Mfsd2a and Spns2 deficiency can be restored after treating with ASP4058 and S1P (fig. S9, F and G), and it is meaningful for manipulating the BBB.

S1P influences the formation of the BBB in embryos

The BBB is gradually disrupted when the concentration of S1P is gradually reduced in adults. We next determined whether the S1P concentration contributes to the development of the BBB in embryos. The expression of Mfsd2a in the endothelium of the brain begins at embryonic day 15.5 (E15.5) (*11*). To confirm the correlation between S1P and BBB integrity, we detected the expression of S1P1 and calprotectin in embryonic brains, and it was found that they are highly expressed at E15.5 (fig. S10), which is consistent with the formation of the BBB. Because injecting FTY720 into pregnant mice at E14.5 and E15.5 results in high embryo mortality, we began continuous administration for 4 days at E16.5 (Fig. 6, A and B). Both Evans blue staining and the 10-kDa dextran tracer showed BBB breakdown (Fig. 6, B and C), indicating that FTY720 interferes with BBB integrity during the embryonic stage. We also found that a proportion of calprotectin dissociated into S100A8 and S100A9 after FTY720 injection (Fig. 6D), which is consistent with the above results. Previous studies have reported that Mfsd2a-deficient embryos have no capability to form an intact BBB; therefore, we tested the S1P concentration in the embryos. The decreased S1P concentration in the ECM in Mfsd2a-deficient embryos suggests that Mfsd2a deficiency leads to the inefficient export of S1P (Fig. 6E). Compared with wild-type embryos, both FTY720-dosed embryos and Mfsd2a-deficient embryos had unstable calprotectin in brain ECs (Fig. 6F). These results suggest that variation in the S1P concentration influences the formation of the BBB.

DISCUSSION

The formation and maintenance of the BBB allows the brain to establish and maintain the functioning of its neural circuits. In ECs, when TJs are disrupted, transcytosis is impaired, and BBB breakdown causes the increased extravasation of peripheral blood cells and toxins and the poor regulation of ionic flux (*1*). Notably, recent studies have reported that S1P plays a potential role in BBB integrity (*37*, *41*). By inhibiting Spns2 and S1P1 in the brain, we provide new evidence that S1P can directly influence the BBB without the need for mediation by peripheral immune cells. Our current study suggests that for ECs in the brain, an S1P-enriched microenvironment is critical for building an intact BBB. The development and leakage of the BBB are not transient events but rather gradual processes (*34*). In addition, we demonstrate that a change in the S1P concentration in the ECM from low to high is a key factor in this process.

In addition, these findings reveal the mechanism by which brain ECs regulate the S1P concentration in the microenvironment via Mfsd2a and Spns2. As the major transporter of S1P in ECs, Spns2 transports S1P from inside cells into the ECM, and Mfsd2a improves the transport efficiency by trapping S1P in membrane, although Mfsd2a has no ability to transport S1P directly. We conclude that a protein complex of Mfsd2a and Spns2 can improve the efficiency of S1P transport in brain ECs. Efficient transport by Spns2 and Mfsd2a maintains a high concentration of S1P in the endothelial ECM, which is essential for the formation and maintenance of the BBB. We hypothesized that the concentrations of S1P in the ECM of the brain are regulated by Spns2 and Mfsd2a and can be divided into three grades: extremely low, low, and high. High concentration of S1P maintains the BBB integrity, low concentration (Mfsd2a-deficient) increases permeability of ECs and promotes transcellular trafficking, and extremely low concentration (Spns2-deficient) further causes opening of TJs. Moreover, this work demonstrates that BBB breakdown caused by a low-concentration S1P is reversible, and the disruption or integrity of the BBB can change at low or high

concentrations of S1P. Revealing the mechanism by which Mfsd2a regulates S1P transport to manipulate the BBB suggests a new therapeutic strategy that could be used for cerebrovascular disorders and also provides a novel method for BBB manipulation to implement drug delivery to the CNS. This finding also highlights the process by which S1P signaling influences calprotectin in brain ECs, which merits further study.

MATERIALS AND METHODS

Animals

All animal experiments followed the National Institutes of Health (NIH) Guide for the Care and Use of Laboratory Animals (NIH publication no. 8023, revised 1978) and were approved by the Animal Ethics Committee of the Fudan University. The mice used in the experiments are on the C57BL6/J background. *Mfsd2a-CreERT2* mice were crossed with *rosa26-LSL-RFP* mice for labeling Mfsd2a-positive cells in brain, which was described previously. By formulating tamoxifen (tam) (20 mg/ml) solution with corn oil, and tam (0.15 mg/g) was injected by oral gavage to induce Mfsd2a-positive cells to express RFP reporter. Ten-week-old male mice were used as adult mice in this study.

Genomic PCR

To obtain the genomic DNA of the mice, tails were collected and then lysed in lysis buffer with proteinase K for 12 hours at 55°C. The tissues were centrifuged at 12,000 rpm for 8 min to collect supernatants. The supernatant was transferred to isopropanol for DNA precipitation, the DNA was washed with 70% ethanol, and the DNA was dissolved in deionized water. rosa26-LSL-RFP: primers 5′-GGCATTAAAG-CAGCGTATCC-3′ and 5′-CTGTTCCTGTACGGCATGG-3′; Mfsd2a-CreER^{T2}: primers 5′-TGATGG GGATTCAGAAGTCAAGG-3′ and 5′-GGACAGAAGCATTTTCCAGGTATG-3′; wild type: primers 5′-CCCCTTTCCTGGGTTGTAAAATG-3′ and 5′-GGGCTTCAGA CTTTCTCCATCAC-3′. All primers were reported previously (*6*).

BBB leakage tests

Twenty microliters of 10-kDa dextran tracer tetramethylrhodamine (4 mg/ml; Invitrogen, D3312) or 200 μl of Evans blue staining (2%; Aicon Biotech, A28136) was injected into adult mice by cardiac perfusion. Two microliters of 10-kDa dextran tracer or 10 μl of Evans blue staining was injected in embryos through the liver (*11*). For dextran tracer, brains were harvested after 5-min circulation and then fixed by 4% paraformaldehyde (PFA) overnight. For Evans blue staining, the mice were transcardially perfused after 10-min circulation, and then the brains were dissected. The tissues stained with Evans blue staining were homogenized in 1000 μl of PBS, sonicated, and centrifuged for 30 min (15,000 rpm). The supernatant was collected, adding 500 μl of 50% trichloroacetic acid for 12 hours at 4°C, and then centrifuged (30 min, 15,000 rpm, 4°C). Evans blue staining was measured by Colibri (Titertek-Berthold) at 610 nm.

S1P extraction and measurement

Five mg of tissue was transferred into a silicified glass tube, cut into 1-mm^3 pieces and incubated in 0.4 ml of PBS at 4°C. After 20 min, the supernatant was separated from the tissue fragments, and the tissue fragments were again homogenized in 0.4 ml (1:1) of methanol/water. The internal standard [C18 (d18:1/18:0) ceramide, (d18:1) sphingosine, and (d18:1/18:0) sphingomyelin; 2 ng each] was added to all samples. Standard lipids were obtained from Sigma-Aldrich (860518P, 860490P, and 860586P). Chloroform (0.4 ml) was added to all samples, vortexed for 1 min, kept on ice for 10 min, and centrifuged at 1000*g* for 5 min. The chloroform layer was removed and dried under a stream of nitrogen. Then, 100 μl of ethanol was added to the samples for reconstitution. The S1P in samples and standard were determined on high-performance liquid chromatography (LC-20AD HPLC) coupled with MS (AB Sciex QTRAP 6500 MS), operated in multiple reaction monitor mode, and the transition was 378.2/79. For quantitative analysis, the concentrations of S1P were calculated as follows: $C_{S1P} = C_{standard} \times (sample\ peak\ area/IS\ peak\ area)$; IS, internal standard.

S1P measurement by ELISA

The standard wells were each added with 50 μl of different concentrations of the standard; the sample wells were first added with 10 μl of the sample to be tested, and then 40 μl of the sample dilution was added. In addition to the blank wells, 100 μl of HRP-conjugated reagent was added to each well, and the reaction wells were sealed with sealing plates and incubated at 37°C for 60 min. We discarded the liquid, patted them dry on the absorbent paper, filled each well with the washing solution, let them stand for 1 min, removed the washing solution, patted them dry on the absorbent paper, and repeated the washing five times. Fifty microliters of each of the substrates A and B were added to each well and incubated at 37°C for 15 min in the dark. Fifty microliters of the stop solution was added to each well, and the optical density (OD) value of each well was measured at a wavelength of 450 nm within 15 min. In the Excel worksheet, the standard concentration was used as the abscissa, and the OD value was plotted as the ordinate. The linear regression curve of the standard was drawn, and the concentration values of each sample were calculated according to the curve equation.

Recombinant DNA

Guide RNA (Mfsd2b) was the following: GGCAAGTGACACCTGG-GCAG NGG. Plasmids were as follows: GV362 (Shanghai GeneChem); CMV-Mfsd2a-3FLAG-IRES-EGFP-SV40-Neomycin (Shanghai GeneChem); CMV-Spns2-IRES-EGFP-SV40-Neomycin (Shanghai GeneChem); CMV-Mfsd2a-IRES-Spns2-SV40-Neomycin (Shanghai GeneChem). Plasmids were transduced into HEK293 cell line by Attractene Transfection Reagent (Qiagen, 301005). AAV, S1P, ASP4058 (1 μg/g; no. HY-111021, MCE), or PBS was injected into the brain by stereotactic injection (injection site: hippocampus, 2 mm to the back of the bregma, 1.5 mm to the left/right of the sagittal suture, 3-mm depth; corpus callosum, 2 mm to the back of the bregma, 1.5 mm to the left/right of the sagittal suture, 1.5-mm depth).

Immunofluorescence staining

Mice were perfused with PBS and 4% PFA. The brains were collected and then bathed in 4% PFA for 90 min, then washed with PBS. Sucrose (30%) in PBS was used to dehydrate, and the tissues were embedded with optimal cutting temperature (OCT; Sakura) compound. The brains were cut into 20-μm sections on a cryostat. The cryosections were air-dried for 40 min at room temperature and then incubated in PBS with 3% donkey serum and 0.1% Triton X-100 for 30 min. Primary antibodies were applied, and the sections were incubated overnight at 4°C, followed by washing with PBS three times. Cryosections were stained with secondary antibodies for 30 min at room temperature, washed by PBS, and lastly counterstained with mounting

media (Vector Laboratories). All samples with fluorescence reporters were observed and photographed on a Nikon (A1+) confocal microscope.

Primary antibodies were as follows: S1P1 (rabbit, 1:100; ab11424, Abcam), Spns2 (rabbit, 1:100; PA5-48915, Invitrogen), Sphk1 (rabbit, 1:100; PA5-28584, Invitrogen), S100A8 (rabbit, 1:100; ab92331, Abcam), S100A9/calprotectin (mouse, 1:200; ab22506, Abcam), glyceraldehyde-3-phosphate dehydrogenase (GAPDH) (rabbit, 1:1000; ab181602, Abcam), Mfsd2a (rabbit, 1:1000; ab105399, Abcam), glial fibrillary acidic protein (chicken, 1:800; ab4674, Abcam), S100β (rabbit, 1:400; ab52642, Abcam), vascular endothelial cadherin (VE-cad) (goat, 1:100; AF1002, R&D), Claudin-5 (mouse, 1:200; 35-2500, Invitrogen), Isolectin GS-IB4 (1:500; I221411, Invitrogen), FLAG (rabbit, 1:200; ab205606, Abcam). Secondary antibodies: donkey anti-rabbit immunoglobulin G (IgG) heavy chain and light chain (H&L) Alexa Fluor 488 (1:1000; ab150073, Abcam), donkey anti-goat IgG H&L Alexa Fluor 488 (1:1000; ab150129, Abcam), goat anti-chicken IgY H&L Alexa Fluor 488 (1:1000; ab150169, Abcam), donkey anti-mouse IgG H&L Alexa Fluor 488 (1:1000; ab150105, Abcam), donkey anti-rabbit IgG H&L Alexa Fluor 555 (1:1000; ab150074, Abcam), donkey anti-rat IgG H&L Alexa Fluor 555 (1:1000; ab150154, Abcam), donkey anti-rabbit IgG H&L Alexa Fluor 647 (1:1000; ab150075, Abcam) donkey anti-goat IgG H&L Alexa Fluor 555 (1:1000; ab150130, Abcam), and donkey anti-mouse IgG H&L Alexa Fluor 647 (1:1000; ab150107, Abcam).

Immunoprecipitation and S1P binding

Immunoprecipitation was performed by following the instructions of the Pierce Co-Immunoprecipitation Kit (no. 26149, Thermo Fisher Scientific). After Mfsd2a-FLAG bound to columns, 0.5 ml of S1P (1 μM) dissolved in PBS was added per column. They were incubated for 1 hour and the resin was washed three times with 300 μl (1:1) of methanol/water. Twenty μl of elution buffer was added to obtain Mfsd2a and S1P.

Flow cytometry sorting

Mice were anesthetized with isoflurane, perfused with 4°C PBS, and decapitated. Tissues were collected and cut into small pieces and then digested by 1 ml of collagenase (0.2 mg/ml) for 15 min at 37°C, supplemented with deoxyribonuclease I (0.1 mg/ml). We added 1 ml of PBS with 10% fetal bovine serum to block collagenase. Mixture was filtered through a 40-μm filter and resuspended in PBS [0.5% bovine serum albumin (BSA)]. The cells were stained with primary antibody mouse anti-CD31 (ab9498, Abcam) for 30 min at 4°C, washed with 500 μl of PBS, and centrifuged (300*g*) for 3 min to collect cells. The secondary antibody was subjected to the same process for staining and washing as above, resuspending the cells in 500 μl of PBS with 0.15% BSA for sorting (BD FACSCalibur). The data were analyzed by FlowJo (v7.6) software (Tree Star).

Quantitative RT-PCR

The brain tissues or cells were lysed by TRIzol reagent (Invitrogen) and total RNA extraction followed the manufacturer's instructions (Invitrogen). RNA was converted to complementary DNA (cDNA) by PrimeScript reverse transcription (RT) kit (TaKaRa). SYBR Green quantitative polymerase chain reaction Master Mix (Applied Biosystems) was used, and cDNA was amplified on a StepOnePlus real-time PCR system (Applied Biosystems). Primers are listed below:

α-tubulin: forward, 5′-TGTGGCAGGACTCTGGTTAG-3′; reverse, 5′-CCATCTTCG AGCACATAGCG-3′; cav-1: forward, 5′-CGACCCTAAACACCTCAACGA-3′; reverse, 5′-TCCCTTCTGGTTCTGTCA-3′; cav-2: forward, 5′-AGGATGGTACTTAG GTGGTGTGT-3′; reverse, 5′-GTAACAGCCCAGTTGGTAAACAAA-3′; cav-3: forward, 5′-CCAAGAACATCAATGAGGACATTGTG-3′; reverse, 5′-GTG GCA GAA GGA GAT ACAG-3′; Tlr4: forward, 5′-AAT CCC TGC ATA GAG GTA GTT CC-3′; reverse, 5′-GTCTCCACAGCCACCAGATT-3′; FcRn: forward, 5′-CTGACCTG TGCTGCTTTCTC-3′; reverse, 5′-GCTCATCTCCACGTTTGACC-3′; reverse, 5′-CCCGGAGCCTGAGGCTAGCCC-3′; Rab5: forward, 5′- GAGCTCCTGTGCAAGA AAGG-3′; reverse, 5′-GAAGTCGTTCTGCCAGTTCC-3′; forward, 5′-CGGCAACCCTGCCTGGCAGG-3′; Rab7: forward, 5′-CTGACCAAGGAGGTGATGGT-3′; reverse, 5′-ACCTCTGTAGAAGGCCACAC-3′; forward, 5′-ACCGGCTGTGTCCCA GATCTGCA-3′; Rab9: 1 forward, 5′-AGGACGTCCAGTGTGTGTCT-3′; reverse, 5′-AGTGAGTGTCCCTTCTCCCA-3′; 2 forward, 5′-ATTGGTTCTTCTGCCCCAGTC-3′; reverse, 5′-CCGGTAAAATGGCGTCCTCA-3′; Rab28: forward, 5′-CCTCGGGGAAGACCTCC TTA-3′; reverse, 5′-TAAAGCAACCAGGGGCTGAG-3′; GAPDH: forward, 5′-TGGAAGATGGTGATGGGCTT-3′; reverse, 5′-ACAAGCTT GGCATTCAGCAA-3′.

Western blotting

Brain tissues or cells were isolated with radioimmunoprecipitation assay (Sigma-Aldrich) buffer supplemented with Protease Inhibitor Cocktail (Roche). After centrifugation to separate lysates from the supernatant, proteins were separated using SDS–polyacrylamide gel electrophoresis (PAGE), followed by transfer to a nitrocellulose membrane. For Native-PAGE, proteins were extracted by Non-denature Lysis Buffer (Sangon Biotech, C510013) and separated using Precast-GLgel Hepes Native-PAGE (BBI, C601100). The nitrocellulose membranes were immersed with primary antibodies (see above), followed by secondary antibodies conjugated with HRP. Secondary antibodies are listed below:

goat anti-rabbit IgG H&L (HRP) (1:2000; ab6721, Abcam), goat anti-mouse IgG (1:5000; A0216, Beyotime), and goat anti-rabbit IgG (1:5000; A0208, Beyotime).

Transmission electron microscopy

Transmission electron microscopy (TEM) imaging of cortical capillaries by HRP injection was performed as previously described (*11*). HRP [10 mg (per 20 g); Sigma-Aldrich, HRP type II] was dissolved in 0.4 ml of PBS and injected into the tail vein of deeply anesthetized P90 mice. After 30 min of HRP cycle, the brain was dissected and fixed by soaking in 5% glutaraldehyde for 1 hour at room temperature and then soaking in PFA for 5 hours at 4°C. After fixation, the tissue was washed overnight in 0.1 M sodium cacodylate buffer and then cut in a 50-mm-thick free-floating section using a vibratome. The sections were incubated for 45 min at room temperature in 0.05 M tris-HCl (pH 7.6) buffer containing 5.0 mg/10 ml of 3′3-diaminobenzidine (DAB; Sigma-Aldrich) containing 0.01% hydrogen peroxide. The sections were then fixed in 1% osmium tetroxide and 1.5% potassium ferrocyanide, then dehydrated, and embedded in an epoxy resin. Ultrathin sections were stained with Reynolds lead citrate and examined under an electron microscope (FEI Tecnai G2) equipped with a 2.5k charge-coupled device digital camera (Advanced Microscopy Techniques).

Behavior tests

Behavior tests were carried out by two observers who were blinded to mouse conditions, with odor eliminated with alcohol. All behavior

tests were performed at postnatal 70 days (P70). For the open-field test, the apparatus included a central area (30 cm by 30 cm) within a square black box (60 cm by 60 cm by 25 cm). Mice were placed in the black box for 20 min, and their behavior was recorded on video. The open-field test is based on the concept that mice prefer to be near a protective wall rather than exposing themselves to the danger of an open field. For the rotarod test, the spin velocity of the apparatus was gradually accelerated to 40 rpm. The time at which the mouse fell from the rotarod apparatus was recorded. Before the test, the mice were trained to adapt to the rotating rod and mice with similar fall time were selected for experimentation. The novel object recognition test was performed as previously described (*12*). Briefly, mice were trained for 5 min with the same "familiar" object and then assessed for short-term memory and long-term memory, 30 min and 24 hours after training, respectively. The preference score is calculated as (exploring times for new object − exploring times for familiar object)/(exploring the total number of two objects). The preference for familiar objects and new objects is defined as a negative score, and a score close to zero means no preference for either object.

Statistical analysis

The data are presented as means ± SEM. Cell counting was performed using ImageJ (NIH). All data were analyzed with independent-samples *t* tests using Prism 6 (GraphPad). $*P < 0.05$, $**P < 0.01$, $***P < 0.001$, and $****P < 0.0001$ were considered statistically significant.

SUPPLEMENTARY MATERIALS

Supplementary material for this article is available at http://advances.sciencemag.org/cgi/content/full/6/22/eaay8627/DC1

View/request a protocol for this paper from *Bio-protocol*.

REFERENCES AND NOTES

1. B. Obermeier, R. Daneman, R. M. Ransohoff, Development, maintenance and disruption of the blood-brain barrier. *Nat. Med.* **19**, 1584–1596 (2013).
2. Z. Zhao, A. R. Nelson, C. Betsholtz, B. V. Zlokovic, Establishment and dysfunction of the blood-brain barrier. *Cell* **163**, 1064–1078 (2015).
3. B. V. Zlokovic, Neurovascular pathways to neurodegeneration in Alzheimer's disease and other disorders. *Nat. Rev. Neurosci.* **12**, 723–738 (2011).
4. N. J. Abbott, L. Rönnbäck, E. Hansson, Astrocyte-endothelial interactions at the blood-brain barrier. *Nat. Rev. Neurosci.* **7**, 41–53 (2006).
5. P. Oh, P. Borgström, H. Witkiewicz, Y. Li, B. J. Borgström, A. Chrastina, K. Iwata, K. R. Zinn, R. Baldwin, J. E. Testa, J. E. Schnitzer, Live dynamic imaging of caveolae pumping targeted antibody rapidly and specifically across endothelium in the lung. *Nat. Biotechnol.* **25**, 327–337 (2007).
6. B. J. Andreone, B. W. Chow, A. Tata, B. Lacoste, A. Ben-Zvi, K. Bullock, A. A. Deik, D. D. Ginty, C. B. Clish, C. Gu, Blood-brain barrier permeability is regulated by lipid transport-dependent suppression of caveolae-mediated transcytosis. *Neuron* **94**, 581–594.e5 (2017).
7. B. W. Chow, C. Gu, The molecular constituents of the blood-brain barrier. *Trends Neurosci.* **38**, 598–608 (2015).
8. S. Liebner, R. M. Dijkhuizen, Y. Reiss, K. H. Plate, D. Agalliu, G. Constantin, Functional morphology of the blood-brain barrier in health and disease. *Acta Neuropathol.* **135**, 311–336 (2018).
9. M. D. Sweeney, Z. Zhao, A. Montagne, A. R. Nelson, B. V. Zlokovic, Blood-brain barrier: From physiology to disease and back. *Physiol. Rev.* **99**, 21–78 (2019).
10. A. Ben-Zvi, B. Lacoste, E. Kur, B. J. Andreone, Y. Mayshar, H. Yan, C. Gu, Mfsd2a is critical for the formation and function of the blood-brain barrier. *Nature* **509**, 507–511 (2014).
11. L. N. Nguyen, D. Ma, G. Shui, P. Wong, A. Cazenave-Gassiot, X. Zhang, M. R. Wenk, E. L. K. Goh, D. L. Silver, Mfsd2a is a transporter for the essential omega-3 fatty acid docosahexaenoic acid. *Nature* **509**, 503–506 (2014).
12. J. P. Chan, B. H. Wong, C. F. Chin, D. L. A. Galam, J. C. Foo, L. C. Wong, S. Ghosh, M. R. Wenk, A. Cazenave-Gassiot, D. L. Silver, The lysolipid transporter Mfsd2a regulates lipogenesis in the developing brain. *PLOS Biol.* **16**, e2006443 (2018).
13. A. Guemez-Gamboa, L. N. Nguyen, H. Yang, M. S. Zaki, M. Kara, T. Ben-Omran, N. Akizu, R. O. Rosti, B. Rosti, E. Scott, J. Schroth, B. Copeland, K. K. Vaux, A. Cazenave-Gassiot, D. Q. Y. Quek, B. H. Wong, B. C. Tan, M. R. Wenk, M. Gunel, S. Gabriel, N. C. Chi, D. L. Silver, J. G. Gleeson, Inactivating mutations in MFSD2A, required for omega-3 fatty acid transport in brain, cause a lethal microcephaly syndrome. *Nat. Genet.* **47**, 809–813 (2015).
14. V. Alakbarzade, A. Hameed, D. Q. Y. Quek, B. A. Chioza, E. L. Baple, A. Cazenave-Gassiot, L. N. Nguyen, M. R. Wenk, A. Q. Ahmad, A. Sreekantan-Nair, M. N. Weedon, P. Rich, M. A. Patton, T. T. Warner, D. L. Silver, A. H. Crosby, A partially inactivating mutation in the sodium-dependent lysophosphatidylcholine transporter MFSD2A causes a non-lethal microcephaly syndrome. *Nat. Genet.* **47**, 814–817 (2015).
15. R. L. Proia, T. Hla, Emerging biology of sphingosine-1-phosphate: Its role in pathogenesis and therapy. *J. Clin. Investig.* **125**, 1379–1387 (2015).
16. Z. Zhao, B. V. Zlokovic, Blood-brain barrier: A dual life of MFSD2A? *Neuron* **82**, 728–730 (2014).
17. S. Spiegel, S. Milstien, Functions of the multifaceted family of sphingosine kinases and some close relatives. *J. Biol. Chem.* **282**, 2125–2129 (2007).
18. S. Spiegel, S. Milstien, The outs and the ins of sphingosine-1-phosphate in immunity. *Nat. Rev. Immunol.* **11**, 403–415 (2011).
19. S. Spiegel, S. Milstien, Sphingosine-1-phosphate: Signaling inside and out. *FEBS Lett.* **476**, 55–57 (2000).
20. R. W. Y. Liu, T. Yamashita, Y. Mi, C.-X. Deng, J. P. Hobson, H. M. Rosenfeldt, V. E. Nava, S. S. Chae, M.-J. Lee, C. H. Liu, T. Hla, S. Spiegel, R. L. Proia, Edg-1, the G protein–coupled receptor for sphingosine-1-phosphate, is essential for vascular maturation. *J. Clin. Invest.* **106**, 951–961 (2000).
21. K. Mizugishi, T. Yamashita, A. Olivera, G. F. Miller, S. Spiegel, R. L. Proia, Essential role for sphingosine kinases in neural and vascular development. *Mol. Cell. Biol.* **25**, 11113–11121 (2005).
22. K. Yanagida, C. H. Liu, G. Faraco, S. Galvani, H. K. Smith, N. Burg, J. Anrather, T. Sanchez, C. Iadecola, T. Hla, Size-selective opening of the blood-brain barrier by targeting endothelial sphingosine 1-phosphate receptor 1. *Proc. Natl. Acad. Sci. U.S.A.* **114**, 4531–4536 (2017).
23. A. Huwiler, U. Zangemeister-Wittke, The sphingosine 1-phosphate receptor modulator fingolimod as a therapeutic agent: Recent findings and new perspectives. *Pharmacol. Ther.* **185**, 34–49 (2018).
24. R. Cipriani, J. C. Chara, A. Rodríguez-Antiguedad, C. Matute, FTY720 attenuates excitotoxicity and neuroinflammation. *J. Neuroinflammation* **12**, 86 (2015).
25. W. Pu, H. Zhang, X. Huang, X. Tian, L. He, Y. Wang, L. Zhang, Q. Liu, Y. Li, Y. Li, H. Zhao, K. Liu, J. Lu, Y. Zhou, P. Huang, Y. Nie, Y. Yan, L. Hui, K. O. Lui, B. Zhou, Mfsd2a$^+$ hepatocytes repopulate the liver during injury and regeneration. *Nat. Commun.* **7**, 13369 (2016).
26. W. Zhang, H. Zhang, H. Mu, W. Zhu, X. Jiang, X. Hu, Y. Shi, R. K. Leak, Q. Dong, J. Chen, Y. Gao, Omega-3 polyunsaturated fatty acids mitigate blood-brain barrier disruption after hypoxic-ischemic brain injury. *Neurobiol. Dis.* **91**, 37–46 (2016).
27. W. Schubert, P. G. Frank, B. Razani, D. S. Park, C. W. Chow, M. P. Lisanti, Caveolae-deficient endothelial cells show defects in the uptake and transport of albumin in vivo. *J. Biol. Chem.* **276**, 48619–48622 (2001).
28. S. Fukuhara, S. Simmons, S. Kawamura, A. Inoue, Y. Orba, T. Tokudome, Y. Sunden, Y. Arai, K. Moriwaki, J. Ishida, A. Uemura, H. Kiyonari, T. Abe, A. Fukamizu, M. Hirashima, H. Sawa, J. Aoki, M. Ishii, N. Mochizuki, The sphingosine-1-phosphate transporter Spns2 expressed on endothelial cells regulates lymphocyte trafficking in mice. *J. Clin. Invest.* **122**, 1416–1426 (2012).
29. A. Mendoza, B. Bréart, W. D. Ramos-Perez, L. A. Pitt, M. Gobert, M. Sunkara, J. J. Lafaille, A. J. Morris, S. R. Schwab, The transporter Spns2 is required for secretion of lymph but not plasma sphingosine-1-phosphate. *Cell Rep.* **2**, 1104–1110 (2012).
30. J.-H. Paik, A. Skoura, S.-S. Chae, A. E. Cowan, D. K. Han, R. L. Proia, T. Hla, Sphingosine 1-phosphate receptor regulation of N-cadherin mediates vascular stabilization. *Genes Dev.* **18**, 2392–2403 (2004).
31. Y. Jin, E. Knudsen, L. Wang, Y. Bryceson, B. Damaj, S. Gessani, A. A. Maghazachi, Sphingosine 1-phosphate is a novel inhibitor of T-cell proliferation. *Blood* **101**, 4909–4915 (2003).
32. M. L. Allende, T. Yamashita, R. L. Proia, G-protein-coupled receptor S1P1 acts within endothelial cells to regulate vascular maturation. *Blood* **102**, 3665–3667 (2003).
33. N. Burg, S. Swendeman, S. Worgall, T. Hla, J. E. Salmon, Sphingosine 1-phosphate receptor 1 signaling maintains endothelial cell barrier function and protects against immune complex-induced vascular injury. *Arthritis Rheumatol.* **70**, 1879–1889 (2018).
34. B. W. Chow, C. Gu, Gradual suppression of transcytosis governs functional blood-retinal barrier formation. *Neuron* **93**, 1325–1333.e3 (2017).
35. J. M. Ehrchen, C. Sunderkotter, D. Foell, T. Vogl, J. Roth, The endogenous Toll-like receptor 4 agonist S100A8/S100A9 (calprotectin) as innate amplifier of infection, autoimmunity, and cancer. *J. Leukoc. Biol.* **86**, 557–566 (2009).
36. C. Kerkhoff, M. Klempt, V. Kaever, C. Sorg, The two calcium-binding proteins, S100A8 and S100A9, are involved in the metabolism of arachidonic acid in human neutrophils. *J. Biol. Chem.* **274**, 32672–32679 (1999).
37. T. Vogl, K. Tenbrock, S. Ludwig, N. Leukert, C. Ehrhardt, M. A. D. van Zoelen, W. Nacken, D. Foell, T. van der Poll, C. Sorg, J. Roth, Mrp8 and Mrp14 are endogenous activators

of Toll-like receptor 4, promoting lethal, endotoxin-induced shock. *Nat. Med.* **13**, 1042–1049 (2007).
38. A. Rubio-Araiz, F. Porcu, M. Pérez-Hernández, M. S. García-Gutiérrez, M. A. Aracil-Fernández, M. D. Gutierrez-López, C. Guerri, J. Manzanares, E. O'Shea, M. I. Colado, Disruption of blood-brain barrier integrity in postmortem alcoholic brain: preclinical evidence of TLR4 involvement from a binge-like drinking model. *Addict. Biol.* **22**, 1103–1116 (2017).
39. R. Mayerhofer, E. E. Fröhlich, F. Reichmann, A. Farzi, N. Kogelnik, E. Fröhlich, W. Sattler, P. Holzer, Diverse action of lipoteichoic acid and lipopolysaccharide on neuroinflammation, blood-brain barrier disruption, and anxiety in mice. *Brain Behav. Immun.* **60**, 174–187 (2017).
40. Z. He, M. Riva, P. Björk, K. Swärd, M. Mörgelin, T. Leanderson, F. Ivars, CD14 is a co-receptor for TLR4 in the S100A9-induced pro-inflammatory response in monocytes. *PLOS ONE* **11**, e0156377 (2016).
41. D. Zhu, Y. Wang, I. Singh, R. D. Bell, R. Deane, Z. Zhong, A. Sagare, E. A. Winkler, B. V. Zlokovic, Protein S controls hypoxic/ischemic blood-brain barrier disruption through the TAM receptor Tyro3 and sphingosine 1-phosphate receptor. *Blood* **115**, 4963–4972 (2010).

Acknowledgments
Funding: This work was supported by grants (2018YFA0107900, 31771491, NSF81761138040, 81471242, and 81601069) from the National Nature Science Foundation and Ministry of Science and Technology of China. We appreciate Z. Bin of the Shanghai Institutes for Biological Sciences for Mfsd2a-CreERT2 mice. We thank S. Hongying of the Institutes of Brain Science of the Fudan University for providing technical support for mice construction and S. Shuhui for technique support for flow cytometry. **Author contributions:** J. Zhu, B.Z., and Z.W. designed the study. Y.Z. and Z.W. performed these experiments and analyzed the data. J. Zhu conceived the study. F. Ma, Y.Z., T. Zhu., F.W., and Z.W. bred the mice and performed the experiments. Y.Z., J. Zhong, T. Zhao, Q.X., Q.T., and Z.W. provided valuable comments and reagents and edited the manuscript. Z.W. and F.W. analyzed the data and wrote the manuscript. **Competing interests:** The authors declare that they have no competing interests. **Data and materials availability:** All data needed to evaluate the conclusions in the paper are present in the paper and/or the Supplementary Materials. Additional data related to this paper may be requested from the authors.

Submitted 24 July 2019
Accepted 18 March 2020
Published 29 May 2020
10.1126/sciadv.aay8627

Citation: Z. Wang, Y. Zheng, F. Wang, J. Zhong, T. Zhao, Q. Xie, T. Zhu, F. Ma, Q. Tang, B. Zhou, J. Zhu, Mfsd2a and Spns2 are essential for sphingosine-1-phosphate transport in the formation and maintenance of the blood-brain barrier. *Sci. Adv.* **6**, eaay8627 (2020).